Supplement of

Improved slant column density retrieval of nitrogen dioxide and formaldehyde for OMI and GOME-2A from QA4ECV: intercomparison, uncertainty characterization, and trends

Marina Zara et al.

Correspondence to: Marina Zara (marina.zara@knmi.nl)

S1. Disentanglement scheme to investigate NO_2 SCD uncertainty dependencies

The statistical NO_2 SCD uncertainty decreases with increasing SCD, most notably for OMNO2-NASA. To further investigate whether SCD uncertainty reduction is driven by the SCD itself ("more signal") or by the top-of-atmosphere reflectance levels ("better signal-to-noise"), we use a 3-step disentanglement scheme wherein our ensemble of Pacific observations 1) are divided in AMF bins, 2) each AMF-bin is divided into SCD sub-bins, and 3) each SCD sub-bin is sliced in low top-of-atmosphere reflectance (R < 0.04) and high top-of-atmosphere reflectance (R > 0.2) boxes. Hereby we can analyze whether SCD uncertainties for low reflectance and high reflectance scenes are significantly different for pixels with very similar AMFs and SCDs.

The distribution of the deviations of the SCDs from the box-mean SCD for the low-reflectance and the high-reflectance scenes with similar AMF and SCD values for OMINO2-QA4ECV is shown in Figure S1. The box-mean AMFs and SCDs used here were 2.25±0.25 and 5±1×10^{15} molec. cm^{-2}, respectively.

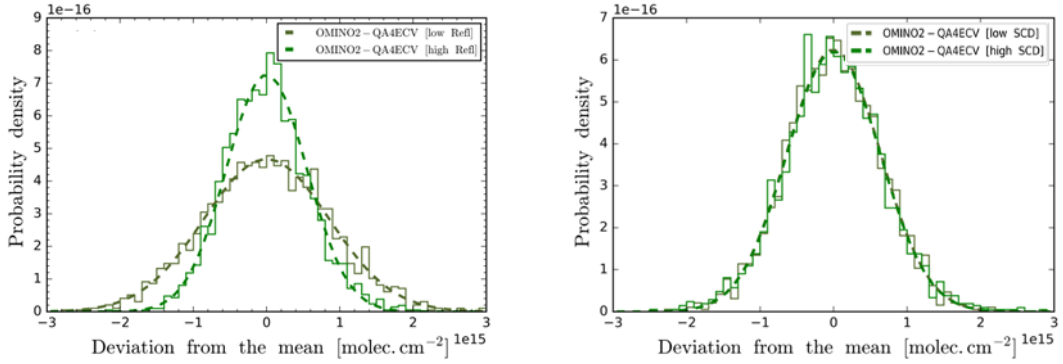

Figure S1. Distribution of the deviation of the OMI NO_2 SCDs from the mean-SCD within [left] low-reflectance (dark-green line) and high-reflectance (light-green line) boxes, and [right] low-SCD (dark-green line) and high-SCD (light-green line) within the same sub-bin in a histogram for OMINO2-QA4ECV.

The NO_2 SCD uncertainties are substantially higher for low-reflectance than for high-reflectance scenes (Table S1). Over bright scenes, the OMINO2-QA4ECV SCD uncertainty is 35% lower than for dark scenes. This suggests that the top-of-atmosphere reflectance is potentially the main SCD-uncertainty driver.

Table S1. Statistical uncertainty estimates of OMI NO_2 SCDs for the OMINO2-QA4ECV algorithm for boxes within the same AMF-bin; boxes in the same SCD sub-bin are divided in low- and high- reflectance boxes (left), and boxes in the same reflectance sub-bin are divided in low- and high- SCD boxes (right).

	OMINO2-QA4ECV SCD uncertainty [molec. cm^{-2}]	[molec. cm^{-2}]	OMINO2-QA4ECV SCD uncertainty [molec. cm^{-2}]
Low-Refl. (<0.04)	0.86 × 10^{15}	Low-SCD (<7×10^{15})	0.64× 10^{15}
High-Refl. (>0.2)	0.55 × 10^{15}	High-SCD (>12×10^{15})	0.64× 10^{15}

We repeat the same procedure to investigate whether SCD uncertainties for low and high SCD values are significantly different for pixels with very similar AMFs and top-of-atmosphere reflectance levels. We create AMF bins and reflectance sub-bins, with low-SCD (SCD < 7×10^{15} molec. cm^{-2}) and high-SCD (SCD > 12×10^{15} molec. cm^{-2}) boxes. The box-mean AMFs and reflectances were 3.75±0.25 and 0.1±0.02, respectively. We see that for OMINO2-QA4ECV the NO_2 SCD uncertainty has the same value for both low- and high- SCD boxes (Table S1), indicating that the SCD uncertainty does not depend on the SCD value. The OMNO2A v2 algorithm

(not shown) yields similar results to OMINO2-QA4ECV for both schemes. OMNO2-NASA uncertainties differ for the low- and high-SCD indicating that they are more sensitive to SCD values (Figure 7a).

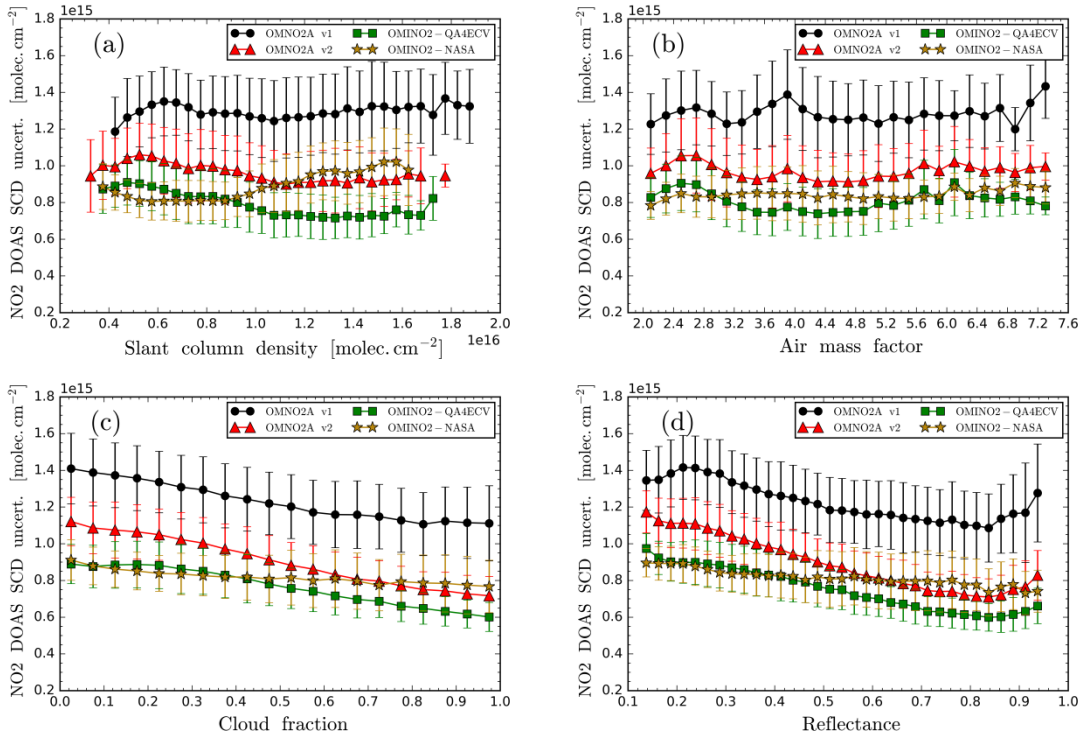

Figure S2. The DOAS OMI NO_2 SCD uncertainty as a function of the (a) SCD, (b) AMF, (c) cloud fraction, and (d) the top-of-atmosphere reflectance for OMNO2A v1 (black circles), OMNO2A v2 (red triangles), OMINO2-QA4ECV (green squares) and OMNO2-NASA (yellow stars) SCDs for the Pacific orbit from day 1 of January, April, July and October (or closest available data) 2005-2015. Each bin contains at least 10 boxes for robust statistics and intercomparisons. The error bars represent one standard deviation (1σ).

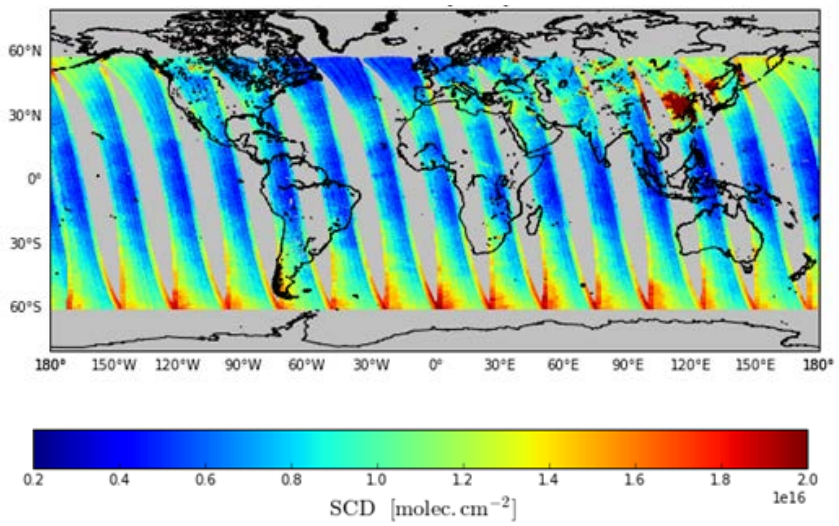

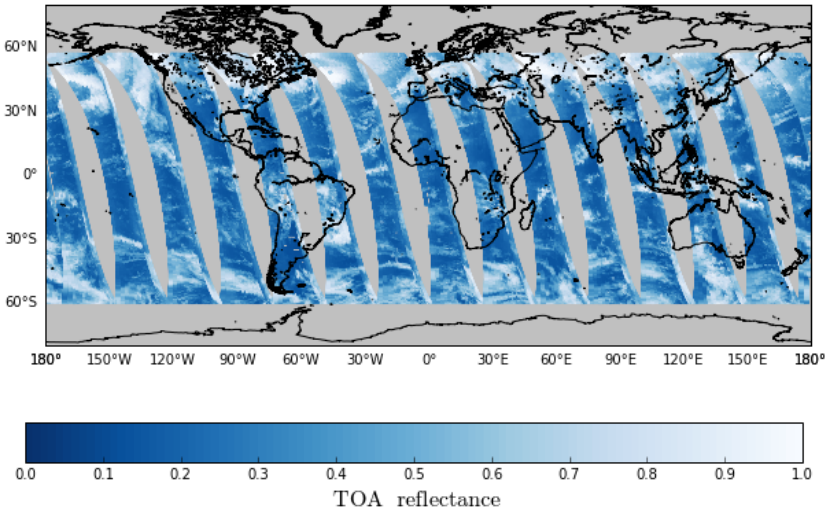

Figure S3. NO_2 SCD (top panel) from OMINO2-QA4ECV and top-of-atmosphere reflectance (bottom panel) on 1 January 2012.

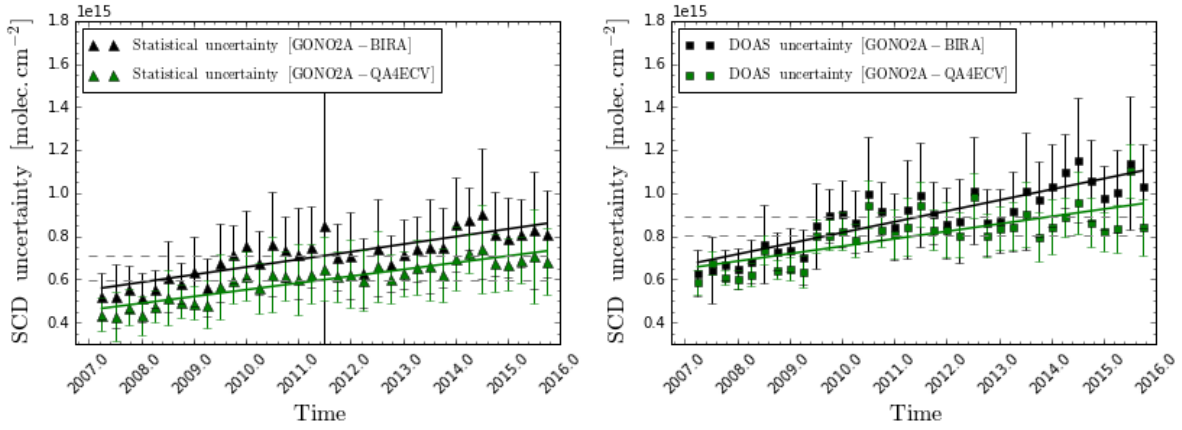

Figure S4. Temporal evolution of the statistical (triangles) and DOAS (squares) GOME-2A NO_2 SCD uncertainty over 2007-2015 (Pacific orbit from day 1 of January, April, August, October- or closest available data) for GONO2A-BIRA (black), and GONO2A-QA4ECV (green) algorithms. Error bars represent one standard deviation (1σ). Solid lines represent the linear regressions fitted to the data for the 9-year period. The slope, p, of each fit on the statistical, p^s, and DOAS uncertainty, p^d, is:

$$p^{\mathrm{s}}_{\mathrm{bira}} = 0.035 \times 10^{15} \pm 0.004 \times 10^{15}\ \mathrm{molec.\,cm^{-2}\ yr^{-1}} \text{ and } p^{\mathrm{d}}_{\mathrm{bira}} = 0.050 \times 10^{15} \pm 0.005 \times 10^{15}\ \mathrm{molec.\,cm^{-2}\ yr^{-1}},$$

$$p^{\mathrm{s}}_{\mathrm{qa4ecv}} = 0.031 \times 10^{15} \pm 0.002 \times 10^{15}\ \mathrm{molec.\,cm^{-2}\ yr^{-1}} \text{ and } p^{\mathrm{d}}_{\mathrm{qa4ecv}} = 0.035 \times 10^{15} \pm 0.006 \times 10^{15}\ \mathrm{molec.\,cm^{-2}\ yr^{-1}}.$$

Table S2. Yearly increase of the statistical and DOAS uncertainty estimates of GOME-2A NO_2 SCDs for GONO2A-BIRA and GONO2A-QA4ECV algorithms for the Pacific orbit from day 1 of January, April, July and October 2007-2015 for all-sky conditions (top panel) and clear-sky conditions (cloud radiance fraction < 0.5) (bottom panel).

SCD uncertainty (all-sky)	GONO2A-BIRA (2007-2015) [yr^{-1}]	GONO2A-QA4ECV (2007-2015) [yr^{-1}]	SCD uncertainty (crf < 0.5)	GONO2A-BIRA (2007-2015) [yr^{-1}]	GONO2A-QA4ECV (2007-2015) [yr^{-1}]
Statistical	6.3%	6.7%		7.2%	6.9%
DOAS	7.4%	5.3%		7.8%	6.8%

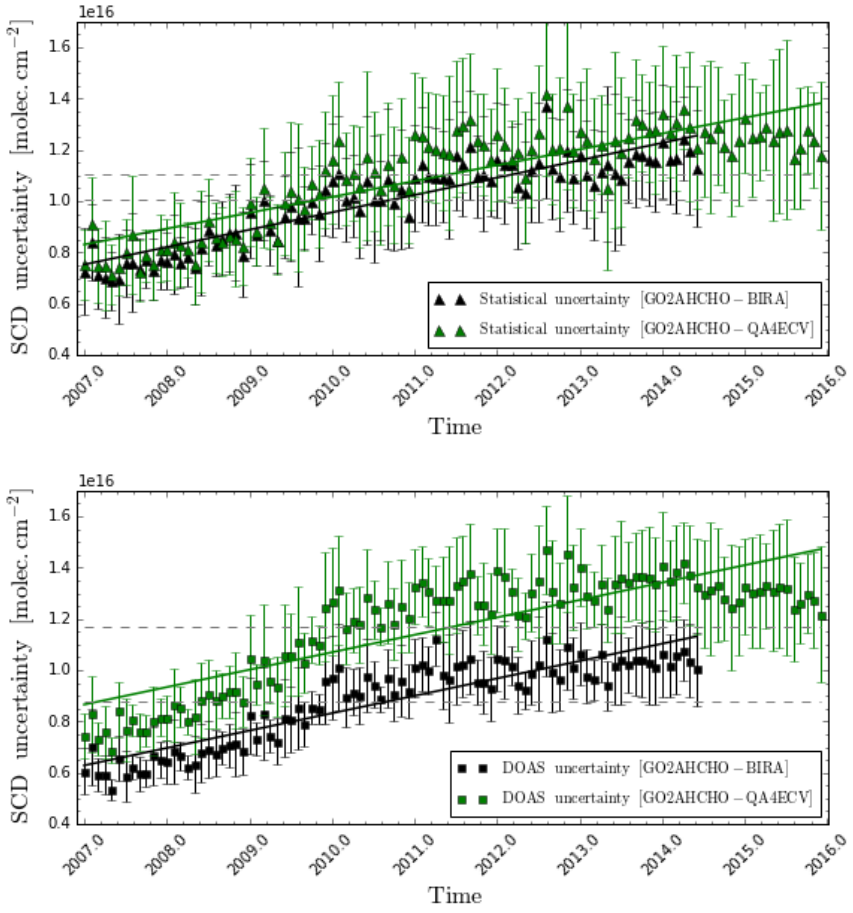

Figure S5. Temporal evolution of the statistical (triangles) and DOAS (squares) GOME-2A HCHO SCD uncertainty over 2007-2015 for GO2AHCHO-BIRA (black) and GO2AHCHO-QA4ECV (green) (Pacific orbit from day 1 of January up to December and from day 15 of January, April, July and October 2007-June 2014 and 2007-2015, respectively). Error bars represent one standard deviation (1σ). Solid lines represent the linear regressions fitted to the data for each period (Table S3). The slope, *p*, of each fit on the statistical, p^s, and DOAS uncertainty, p^d, for GO2AHCHO is: $p^{\mathrm{s}}_{\mathrm{bira}} = 0.68 \times 10^{15} \pm 0.03 \times 10^{15}$ molec. cm^{-2} yr^{-1} and $p^{\mathrm{d}}_{\mathrm{bira}} = 0.68 \times 10^{15} \pm 0.04 \times 10^{15}$ molec. cm^{-2} yr^{-1}, $p^{\mathrm{s}}_{\mathrm{qa4ecv}} = 0.62 \times 10^{15} \pm 0.04 \times 10^{15}$ molec. cm^{-2} yr^{-1} and $p^{\mathrm{d}}_{\mathrm{qa4ecv}} = 0.68 \times 10^{15} \pm 0.04 \times 10^{15}$ molec. cm^{-2} yr^{-1}.

Table S3. Yearly increase of the statistical and DOAS uncertainty estimates of GOME-2A HCHO SCDs for GO2AHCHO-BIRA and GO2AHCHO-QA4ECV (Pacific orbit from day 1 of January up to December and from day 15 of January, April, July and October 2007-June 2014 and 2007-2015, respectively) for all-sky conditions (top panel) and clear-sky conditions (bottom panel). The GO2AHCHO-BIRA data are provided only for scenes with cloud fraction lower than 0.4, therefore the clear-sky conditions yield similar SCD uncertainties to the all-sky conditions.

SCD uncertainty (all-sky)	GO2AHCHO-BIRA (2007-2014) [yr^{-1}]	GO2AHCHO-QA4ECV (2007-2015) [yr^{-1}]	SCD uncertainty (crf < 0.5)	GO2AHCHO-BIRA (2007-2014) [yr^{-1}]	GO2AHCHO-QA4ECV (2007-2015) [yr^{-1}]
Statistical	9.0%	7.4%		10.3%	9.3%
DOAS	10.8%	7.8%		10.8%	9.2%